Low-volume intraplate volcanism in the Early/Middle Jurassic Pacific basin documented by accreted sequences in Costa Rica

David M. Buchs[1], Sébastien Pilet[2], Peter O. Baumgartner[2], Michael Cosca[3], Kennet Flores[4] and Alexandre N. Bandini[5]

[1]GEOMAR, Kiel, Germany (dbuchs@geomar.de)

[2]University of Lausanne, Switzerland

[3]USGS, Denver, USA

[4]American Museum of Natural History, USA

[5]University of Western Australia

This article has been accepted for publication and undergone full peer review but has not been through the copyediting, typesetting, pagination and proofreading process, which may lead to differences between this version and the Version of Record. Please cite this article as doi: 10.1002/ggge.20084

ABSTRACT

Countless seamounts occur on Earth that can provide important constraints on intraplate volcanism and plate tectonics in the oceans, yet their nature and origin remain poorly known due to difficulties in investigating the deep ocean. We present here new lithostratigraphic, age and geochemical data from Lower/Middle Jurassic and Lower Cretaceous sequences in the Santa Rosa accretionary complex, Costa Rica, which offer a valuable opportunity to study a small-sized seamount from a subducted plate segment of the Pacific basin. The seamount is characterized by very unusual lithostratigraphic sequences with sills of potassic alkaline basalt emplaced within thick beds of radiolarite, basaltic breccia and hyaloclastite. An integration of new geochemical, biochronological and geochronological data with lithostratigraphic observations suggests that the seamount formed ~175 Ma ago on thick oceanic crust away from subduction zones and mid-ocean ridges. This seamount travelled ~65 Ma in the Pacific before accretion. It resembles lithologically and compositionally "petit-spot" volcanoes found off Japan, which form in response to plate flexure near subduction zones. Also, the composition of the sills and lava flows in the accreted seamount closely resembles that of potassic alkaline basalts produced by lithosphere cracking along the Line Islands chain. We hypothesize based on these observations, petrological constraints and formation of the accreted seamount coeval with the early stages of development of the Pacific plate that the seamount formed by extraction of small volumes of melt from the base of the lithosphere in response to propagating fractures at the scale of the Pacific basin.

1. Introduction

Countless seamounts occur in the oceans, which can form by thermally-driven processes and the presence of deep mantle plumes, or tectonically-driven processes and fissure propagation in the lithosphere. Seamounts provided important constraints on intraplate

volcanism and plate tectonics in the last decades, but our current knowledge relies essentially on the study of very large volcanoes (tall seamounts or ocean islands), whereas ~90% of the seamounts are <500 m tall and difficult to chart and sample in the deep ocean [Hillier and Watts, 2007; Wessel et al., 2010]. Small-sized seamounts are a major but poorly understood feature on Earth, and remain to be studied in detail. A particular example of small-sized seamount consists of "petit-spot" volcanoes that form in response to plate flexure close to subduction zones [*Hirano et al.*, 2006, 2008; *Valentine and Hirano*, 2010]. However, it remains unconstrained whether these volcanoes are common along subduction zones or occur elsewhere on the ocean floor. The morphology of the ocean floor and age patterns of intraplate volcanism in the Pacific basin over the last 120 Ma suggest that lithosphere cracking is an important process leading to seamount formation [*Natland and Winterer*, 2005], but the contribution of this mechanism in the formation of small-sized seamounts remains poorly constrained. We present here new data on Lower/Middle Jurassic and Lower Cretaceous ocean floor sequences exposed in the Santa Rosa accretionary complex (SRAC, [*Baumgartner and Denyer*, 2006]) in Costa Rica. These sequences allow study of the stratigraphy, composition and mode of formation of a small-sized seamount that formed in the Jurassic, most probably on the now disappeared Farallon Plate. We outline lithological and compositional similarities between the accreted seamount, petit-spot volcanoes and unusual lavas of the Line Islands chain, which provide new insight into the formation of small-sized seamounts or low-volume intraplate volcanism in the ocean.

2. Geological framework

The Santa Rosa accretionary complex is the oldest accretionary complex exposed in the outer forearc of the Middle American margin, and presents direct access to fragments of ancient intraplate oceanic volcanoes [*Hauff et al.*, 2000; *Hoernle et al.*, 2002; *Buchs et al.*,

2011]. The SRAC represents an autochthonous basement of the Santa Elena peninsula (northern Costa Rica) upon which sits a nappe of serpentinized peridotite emplaced during Cenomanian-early Campanian time [*Tournon*, 1994; *Baumgartner and Denyer*, 2006]. Tectonic windows in the nappe expose lithologically distinct accreted assemblages affected by low-grade metamorphic overprinting (Figure 1). A majority of the complex comprises alkaline basalt that occurs both as km-thick composite units of massive and pillowed lava flows and thinner units in which early-middle Pliensbachian to early Toarcian radiolarites are intruded by alkaline basalt sills [*Meschede and Frisch*, 1994; *Tournon*, 1994; *Baumgartner and Denyer*, 2006; *Hauff et al.*, 2000; *Bandini et al.*, 2011a]. The successions of alkaline basalt have previously been interpreted as an Early Jurassic-Late Cretaceous accreted seamount genetically unrelated to other accreted sequences in Central America [*Tournon*, 1994; *Hauff et al.*, 2000; *Geldmacher et al.*, 2008]. Most of the accreted seamounts exposed in Central America may have formed at the paleo-Galapagos Hotspot [*Hoernle et al.*, 2002], but older ages and distinct isotopic composition of seamount sequences in the SRAC clearly indicate a different origin for these sequences. We combine here existing data with new field observations, geochronological data and petrochemical data to better characterize the tectonostratigraphy, composition and origin of unusual ocean floor sequences exposed in the SRAC.

3. Methods

3.1. Bulk rock analyses

Major and trace element analyses were performed at the Institute of Mineralogy and Geochemistry, University of Lausanne, Switzerland. Selected chips of bulk rock samples were powdered with a WC mill. 6 grams of Li-tetraborate were added to 1.2 grams of rock powder and fused in a Pt crucible to obtain lithium tetraborate glass beads. Major element abundances were determined on the lithium tetraborate glass beads using a Philips PW2400

X-ray fluorescence spectrometer. Trace element contents were determined using a laser ablation inductively coupled plasma source mass spectrometer (LA-ICP-MS) instrument equipped with a 193 nm ArF excimer laser (Lambda Physik, Germany) interfaced to an ELAN 6100 DRC quadrupole ICP-MS (Perkin Elmer, Canada). Operating conditions of the laser included 170 mJ output energy, 10 Hz repetition rate, and 120 μm ablation pit size. Helium was used as cell gas. Dwell time per isotope ranged from 10 to 20 ms; peak hopping mode was employed. An SRM 612 glass from NIST was used as an external standard. Three ablations per tetraborate glass bead were made to obtain the trace element contents. Supplemental information related to lithium tetraborate glasses analysis by LA-ICP-MS as used in this study are provided in *Buchs et al.* [2010]. The major and trace elements and sampling coordinates of alkaline sills and massif alkaline basalt are reported in Table S1. Major element contents were normalized on volatile free basis before plotting and interpretations.

3.2. Amphibole analyses

Amphiboles were analyzed using a five spectrometer electron microprobe JEOL JXA-8200 at the Institute of Mineralogy and Geochemistry, University of Lausanne, Switzerland. A 15 keV accelerating potential, 15 nA beam current in spot mode were used. All elements were analyzed for 30 s except for K and Na which have been analysed for 15 s. The composition of selected analysis of amphibole from the different sills and massive alkaline lava are reported in Table S2.

3.3. $^{40}Ar/^{39}Ar$ geochronology

The $^{40}Ar/^{39}Ar$ analyses were performed at the USGS in Denver, CO. Individual fragments of fresh basalt approximately 2 mm^3, together with high purity mineral separates of amphibole and sanidine standards were irradiated in two irradiations of 10 and 20 mega watt

hours, respectively, in the central thimble position of the USGS TRIGA reactor using cadmium lining to prevent nucleogenic production of ^{40}Ar. The neutron flux was monitored using Fish Canyon Tuff sanidine, applying an age of 28.20 Ma ± 0.08 Ma (Kuiper et al. 2008) and isotopic production ratios were determined from irradiated CaF_2 and KCl salts. For these irradiations, the following production values were measured: $(^{40}Ar/^{39}Ar)_K = 0$; $(^{36}Ar/^{37}Ar)_{Ca} = 2.764 \times 10^{-4} \pm 2.7 \times 10^{-6}$; and $(^{39}Ar/^{37}Ar)_{Ca} = 6.97 \times 10^{-4} \pm 4.4 \times 10^{-6}$. The irradiated samples and standards were loaded into 3 mm wells within a stainless steel planchette attached to a fully automated ultra high vacuum extraction line constructed of stainless steel. Samples were incrementally degassed and/or fused using a 20W CO_2 laser equipped with a beam homogenizing lens. The gas was expanded and purified by exposure to a cold finger maintained at −140°C and two hot SAES GP50 getters. Following purification the gas was expanded into a Mass Analyser Products 215-50 mass spectrometer and argon isotopes were measured by peak jumping using an electron multiplier operated in analog mode. Data were acquired during 10 cycles and time zero intercepts were determined by best-fit regressions to the data. Ages were calculated from data that were corrected for mass discrimination, blanks, radioactive decay subsequent to irradiation, and interfering nucleogenic reactions. The $^{40}Ar/^{39}Ar$ step-heating diagrams for whole-rocks and separated-amphiboles analysis are given in Table S3.

4. Results

4.1. Lithostratigraphy

The studied sequences crop out in the Santa Rosa tectonic window, where 100 to 300 m-thick, fault-bounded stacks are composed of alternating Lower Cretaceous trench-fill deposits (i.e. material mostly deposited in a trench proximal to a volcanic arc) and Lower/Middle Jurassic volcano-sedimentary successions that define eight tectonic units (Figures 1 and 2). The accreted sequences are moderately deformed with a roughly

subvertical dip, north-south strike and top to the east orientation, consistent with an initial tectonic arrangement of the complex mostly unaffected by post-accretion tectonics. The base of the trench fill deposits includes siliceous-rich radiolarites poor in detritus that grade up-section into hemipelagic sediment with radiolarian-bearing siliceous mudstone interbedded with centimeter-bedded turbidites (Figures 1c and 2e-f). Coarser detrital deposits increase in abundance up-section and consist of polymict breccias with abundant fragments of radiolarite and basalt (Figures 1c and 2g). These breccias may record mass-wasting on the ocean floor or reworking of accreted/subducting sequences. Gradational lithological changes seen in the trench-fill deposits are most consistent with progressive shift from an ocean floor from a pelagic (detritus-poor) setting into a trench (detritus-rich) environment.

Accreted volcano-sedimentary successions that are the focus of this study include: an unusual ~300 m-thick sequence of ribbon-bedded, weakly-deformed radiolarites intruded by numerous basaltic sills; a ~150 m-thick volcanic breccia composed of abundant basalt pebbles or possible pillow fragments, minor blocks of folded radiolarite, with a matrix of finer-grained, altered volcanic fragments, and minor crosscutting basaltic dikes; and a ~100 m-thick sequence of basalt flows (Figures 1b-c and 2a-d). The radiolarites have a siliceous composition without carbonate or significant amounts of clay, hence suggesting deposition in a deep, pelagic environment protected from significant continental input. These observations, combined with compositional and age consistency of igneous and sedimentary samples (see below), support interpretation as single magmatic suite and seamount.

4.2. Composition of the basalts

Petrographic characteristics

Four sills and one lava flow were sampled for analysis (Table S1). The samples have a consistent mineralogy with 2000-200 μm augite, 500-50 μm kearsutite, 500-50 ηm

plagioclase, and 500-50 μm Fe-Ti oxides phenocrysts embedded in a finer-grained matrix of plagioclase, augite, amphibole, Fe-Ti oxides and glass (Figure 3). Few olivine phenocrysts are observed in sample 07-08-03-08. The proportion of phenocrysts varies from ~35 % in alkaline sill 07-08-03-08 corresponding to a cumulative texture with abundant augite, to few crystals in sample 07-08-03-10. The proportion of glass in the matrix varies from ~40% to ~10% among our samples. Apatite is observed as accessory minerals in all samples and forms small euhedral crystals and/or acicular quenched crystals included in the glass. Minor calcite is observed in vesicles in all samples except basalt POCR07-56, or in micro-veinlets in sample POCR07-51. No textural or mineralogical differences were observed between the sills and the massive and vesicular basalt POCR07-57.

Major element characteristics

Major element contents of Santa Rosa rocks define an alkaline trend controlled by moderate degrees of fractionation (MgO=8.96-4.30 wt. %) or mineral accumulation (Figure 4). Mineral accumulation is particularly important for CaO. The CaO content of alkaline sill 07-08-03-08 that contains cumulative augite is 15.66 wt. %, whereas sill 07-08-03-10 without augite phenocrysts has CaO content of only 6.01 wt.%. The degree of differentiation of the rocks is well indicated by MgO and SiO_2 contents, but samples with similar MgO content have a silica difference of ~3 wt.%. TiO_2 content of the sills and massive basalt does not show significant variation (3.29-4.07 wt. %) relative to silica or magnesium contents. Alkali content (Na_2O+K_2O) of Santa Rosa alkaline basalts is similar to that observed in other alkaline ocean island basalts (OIBs) (Figure 4a). Importantly, some of the Santa Rosa sills are characterized by high K_2O content and high K_2O/Na_2O ratio, which are very unusual for oceanic lavas (Figure 4c). Optical observation of the thin sections indicate that, although phenocrysts are generally well-preserved, alkali content may have been influenced by minor alteration of interstitial glass into palagonite or variable alteration of matrix plagioclase

among the samples. Possible alteration effects are nonetheless unclear as no correlation between the apparent degree of alteration and alkali content was observed. Similarly, loss on ignition (LOI) could not be directly related to gain or loss of K_2O or Na_2O. The samples have moderate LOI (between 2.2 and 6.1 wt. %, Table S1), in particular regarding that ~1 wt% of the LOI could be related to amphibole breakdown during calcinations. Thus, the use of optical observation and chemical composition of bulk rock samples cannot determine if the highly variable K_2O contents of the Santa Rosa alkaline basalts (from 1.39 to 3.67 wt.%) reflect distinct melt compositions or various degrees of alteration. To estimate the content of K_2O in the initial melt we use below the composition of fresh amphiboles that crystallized as phenocrysts in these rocks.

K_2O content based on amphibole composition

Fresh amphibole phenocrysts from Santa Rosa sills and lava flow (Figure 3) share a similar composition, including K_2O content (Table S2). An important observation is that these amphiboles have high K_2O content (1.33 to 1.60 wt.%) compared to that of typical low pressure amphiboles in alkaline series for various oceanic islands (average K_2O content: 1.06 ± 0.28 wt. %) (Figure 5). Assuming that all amphiboles reported in Figure 5 crystallized at low pressure (<4 kbar), this difference suggests that the K_2O content of the Santa Rosa melts are higher than in typical alkaline series observed in oceanic setting.

Difficulty in estimating initial K_2O in the alkaline liquid based on K content in fresh amphiboles relates essentially to the choice of appropriate Kds (Kds=solid/liquid partition coefficients). *Pilet et al.* [2010] reported Kds $^{amph/liq}$ for K measured in various intermediate pressure experiments (0.93-1.5 GPa, Figure 6). These Kds vary from ~0.8 to 0.2 as function of liquid composition, temperature, and pressure (see *Pilet et al.* [2010] for a detailed discussion about the dependence of Kds on P-T and liquid composition). To correct for the effects of liquid composition and crystallization temperature, we used the Mg# - Kd $^{amph/liq}$ K

diagram (Figure 6b) and the Mg# measured in amphiboles from Santa Rosa lavas (Mg#=100*[Mg/(Mg+Fe)]). This yielded a range of Kd $^{amph/liq}$ K between 0.8 and 0.4. The effects of pressure of crystallization on Kd $^{amph/liq}$ K were assessed using the K_2O content in amphiboles produced during equilibrium crystallization at various pressures and temperatures from an initial basanitic liquid [*Peter Ulmer*, unpublished data] (Figure 7). Figure 7 shows that the K_2O content in amphiboles (and by extension the Kd $^{amph/liq}$ for K) decreases significantly with decreasing crystallization pressure. Petrographic observations of the Santa Rosa amphiboles (Figure 3) suggest that they represent phenocrysts and micro-phenocrysts formed at low pressure during cooling of alkaline sills or lava flow. Therefore, our previous estimated range for Kd $^{amph/liq}$ K (0.8 - 0.4), based on 0.93-1.5 GPa experiments, is partly biased. Assuming a lower crystallisation pressure, we can restrict our estimate of Kd $^{amph/liq}$ K to 0.4 -0.6 to calculate the K_2O content of Santa Rosa basaltic melts from which the amphiboles crystallized. The results are reported as ranges of K_2O in Figure 4d and show good agreement with high K_2O content measured in two Santa Rosa alkaline rocks. This clearly suggests that pristine composition of the Santa Rosa basalts is characterized by an unusual, high K_2O content. Consistently high K_2O content in amphibole phenocrysts suggests that lower K_2O values in whole rock composition reflect leaching during secondary alteration.

Alkaline basalts observed in oceanic islands are characterized by K_2O/Na_2O ratio of ~0.4 (K_2O/Na_2O average of the OIBs reported in Figure 4 is 0.38 ± 0.23 (1σ)) and only few analyses indicate values close to those measured in Santa Rosa basalts (Figure 4). To our knowledge, consistent observations of potassic alkaline lavas in submarine volcanic rocks are essentially restricted to Late Cretaceous submarine volcanism of the Line Islands chain [*Natland*, 1976; *Davis et al.*, 2002] and recent petit-spot volcanoes off Japan [*Hirano et al.*, 2006]. A similarly high-K lava sample was collected on a Wake seamount [*Natland*, 1976]. Others may occur in Tuamotu and Samoan chains, but data describing these occurrences

remain to be published [*Natland*, pers. com. 2012]. Figure 4 suggests that the Santa Rosa sills and lava flow are similar to "petit-spot" lavas in term of major element composition. They are slightly richer in total alkalies (Na_2O+K_2O) and K_2O than K-rich alkaline basalts from the Line Islands chain, but potential alteration effects on whole rock compositions of both Santa Rosa and Line Islands basalts do not allow clear distinction.

Trace element characteristics

Santa Rosa sills and lava flow are characterized by high incompatible trace element contents (Rb, Ba, U, Th, Nb and LREE) and high La/Yb ratio, with very consistent patterns of immobile elements (Nb, Zr, Hf, Th, REE) (Figure 8). Some variations are seen in Figure 8 for mobile elements (Rb, Ba, K, Sr) that can be controlled by source or alteration effects, but we showed above that some of the high K values and, by extension, the composition of other mobile elements, are probably not significantly affected by secondary alteration. Lower concentrations of incompatible elements in sill sill 07-08-03-08 relative to other Santa Rosa samples relates to the presence of cumulative augite + minor ilmenite, which decreased incompatible trace element contents of the whole-rock, except Ti. Trace element patterns of the Santa Rosa basalts are broadly similar to those of alkaline rocks observed in oceanic islands (Figure 8a). They are clearly distinct from those of off-axis seamounts from the East Pacific Rise [*Niu and Batiza*, 1997] (Figure 8b), which formed on young lithosphere by degrees of partial melting higher than those assumed for OIBs [e.g. *Reynolds and Langmuir*, 2000]. The high Rb, Ba, K contents observed in Santa Rosa alkaline rocks indicate that these samples are distinct from typical OIBs. However, the Santa Rosa sills and lava flow are characterized by normalized multielement patterns very similar to those of the most enriched lavas from the Line Islands chain seamounts (Figure 8c) [*Davis et al.*, 2002]. Trace element contents of moderately fractionated basalts are only distinguished by slightly lower La/Yb ratios (i.e. slope of REE) and more variable Rb/Ba and Ba/Th ratios in the Line Islands chain

lavas relative to Santa Rosa rocks, which could reflect partly distinct source compositions in the two settings. Normalized multielement patterns of the Santa Rosa sills and lava flow are also very similar to those of petit-spot lavas, with notably a similar slope of REE and a positive Ba anomaly. Basalts from these two localities have slightly distinct Pb and Sr contents, possibly indicating minor source differences. In any case, potassic alkaline basalts of Santa Rosa, petit-spot volcanoes in Japan and Line Islands chain share similar Rb, Ba, K characteristics not seen in typical OIBs.

4.3. Geochronological and biochronological data

Amphiboles separated from two basaltic sills yielded $^{40}Ar/^{39}Ar$ plateau ages of 173.9 +/- 0.5 and 177.0 +/- 0.8 Ma (2sd). These amphibole $^{40}Ar/^{39}Ar$ ages and biochronological dating of radiolarites sampled in the volcano substrate and breccias both indicate formation of the basaltic rocks at ~175 Ma (Figures 1c, 9, and 10). A ~110 Ma age of accretion of the studied sequences is indicated by radiolarians found in trench-fill deposits juxtaposed with volcano-sedimentary sequences (Figures 1c, 2 and 10). This age is supported by ^{40}Ar-^{39}Ar step-heating from three basalts, albeit with complex age spectra (Figures 1c and 9). The $^{40}Ar/^{39}Ar$ step heating data from the three whole rock samples likely reflect the combined effects of diffusive Ar loss, K-alteration, and internal ^{39}Ar and ^{37}Ar recoil. The lower laser power steps have higher K-values and younger ages that transition to older ages with lower K-values at slightly higher laser power and finally yielding ages intermediate between these at highest laser powers. These age patterns and K/Ca evolutions suggest K-alteration is being degassed in the low power steps and that effects of Ar recoil are evident throughout the degassing of the samples. Nonetheless, despite the imprecise age information from these samples, the majority of the step heating ages are between 100 and 120 Ma, which are similar to radiolarian fossil ages from the trench-fill deposits. Collectively, the radiolarian ages and the altered basalt $^{40}Ar/^{39}Ar$ ages support accretion of these deposits at ~110 Ma.

5. Discussion

5.1. Nature and origin of the seamount

Three lines of evidence indicate that the accreted volcano-sedimentary sequences represent a small-sized seamount volcanologically and compositionally similar to petit-spot volcanoes found off Japan:

1) The lithostratigraphic arrangement of units 2 to 7 (Figures 1 and 2) are consistent with the occurrence of a small accreted volcanic edifice. Unit 3, which contains thick radiolarite deposits with volcanic sills compositionally similar to nearby lava flow, is likely to represent the substrate of a small-sized seamount. The radiolarites clearly indicate deposition below the Calcite Compensation Depth (CCD). They do not contain reworked shallow-water material or any other type of detrital sediment that commonly occur on the flanks of large seamounts or in steep submarine environments. Thick packages of siliceous ooze (i.e. the unlithified equivalent of the studied radiolarites) can hardly be preserved on top of large seamounts because they are commonly swept by oceanic currents. In addition, the accreted volcano is included within a well-organized, imbricated tectonic section that contains thin layers of trench-fill sediments (Figure 1b-c). This lithologic arrangement is very similar to that of some other accretionary complexes, which formed by repeated off-scrapping of the uppermost layers of the oceanic crust [*Kimura and Ludden*, 1995]. The subduction or accretion of large seamounts is accompanied by severe disruption of the overlying plate and the formation of tectonic mélanges that may locally include blocks of shallow-marine limestone [*Okamura*, 1991; *Matsuda and Ogawa*, 1993]. These do not occur in the SRAC.

2) The lithologic succession of units 3-5 is very similar to that described in small-sized seamounts off Japan [*Fujiwara et al.*, 2007]. Volcanic breccias associated with deformed sediments and subvolcanic intrusions in weakly deformed pelagic sediments (Figure 2a-c) are

unusual volcanic features but not unexpected in association with small-sized volcanoes developing on a thick pelagic sedimentary cover.

3) The composition of the Santa Rosa sills and lava flow are similar to that of petit-spot volcanoes in Japan or surficial volcanic deposits on seamounts of the Line Islands chain (Figures 4 and 8c, d), but clearly distinct from that of off-axis seamounts from the East Pacific Rise [*Niu and Batiza*, 1997] (Figure 8b). Although similar to typical alkaline rocks observed in oceanic islands, the studied alkaline rocks can be distinguished by higher K_2O contents and K_2O/Na_2O ratios (Figure 4c and d). As indicated previously, minor alteration could have affected the composition of the Santa Rosa basalts, but the high K_2O contents observed in amphibole phenocrysts from Santa Rosa compared to that of low pressure amphiboles from ocean island alkaline series further supports unusual high K contents (Figure 4d) and potentially higher K_2O/Na_2O ratios of the Santa Rosa alkaline basalt compared to typical OIBs. In any case, the formation of the basalts requires very low degrees of partial melting (see below) and extrusion of low volumes of lava consistent with the occurrence of an accreted small-sized volcano.

The origin of the seamount can be assessed using time and lithological constraints. Although deformation partly affected the SRAC, lithostructural arrangement of accreted sequences are relatively well organized, with repeated occurrence of similar lithologies with consistent top-to-the-east orientation. This and high consistency of age and geochemical data in the volcano-sedimentary sequences and trench-fill deposits indicate that emplacement of the seamount sequences is unlikely to have occurred by reworking of previously-accreted sequences, but essentially occurred by direct incorporation from the subducting plate. Therefore, the ~65 Ma time span between the formation (~175 Ma) [*this study*] and accretion (~110 Ma) [*Bandini et al.*, 2011a] of the accreted small-sized seamount and expected fast plate motions in the eastern Pacific during this time interval [*Johnston and Borel*, 2007;

Smith, 2007; *van der Meer,* 2012] indicate that the volcanic edifice must have travelled a few thousand kilometres in the ocean prior to its accretion. In addition, radiolarites from the volcano substrate are pure pelagic deposits that lack coarse arc-derived or terrigenous material generally observed close to subduction zones or continental margins. Hence, the volcano did not form close to a subduction zone. Also, thick pelagic deposits in the volcano substrate and the composition of the basalts preclude volcano formation close to a mid-ocean ridge. We deduce from preceding observations that the small-sized seamount formed in a mid-ocean plate setting. This is an important difference with petit-spot volcanoes found off Japan, which indicates that similar seamounts can also form far from subduction zones.

5.2. Petrogenesis of the seamount

Although formed at very different times and areas in the ocean, potassic alkaline basalts of Santa Rosa, the Line Islands chain and Japanese petit-spot volcanoes share similar compositional features, which are very unusual among OIBs and require a particular mode of magma genesis. The occurrence of potassic alkaline basalts in the Line Islands chain has been compared to continental rift zones, where low-volume magmatism can produce similar lavas [*Natland*, 1976; *Davis et al.*, 2002]. These basalts were emplaced during episodic volcanic events along much of the Line Islands chain, and were interpreted to result from decompressional melting of heterogeneous mantle due to diffuse lithospheric extension [*Davis et al.*, 2002]. Similarly, petit-spot volcanoes are considered to form in response to lithosphere cracking close to subduction zones [*Hirano et al.*, 2006]. It was suggested that low-volume magmatism associated with these seamounts is linked to small-scale, fertile recycled plate material that occurs pervasively in the upper mantle [*Machida et al.*, 2009]. Preceding studies provided important contextual and geochemical data on the formation of potassic alkaline basalts in the ocean. To provide new insight into the petrogenesis of the

Santa Rosa basalts (and similar rocks in the ocean) we outline below key petrological aspects that have remained poorly used in previous studies.

The Santa Rosa, Line Islands and Japanese petit-spot alkaline basalts are characterized by high K_2O and TiO_2 contents. These features cannot be accounted for by fractional crystallization process or low degrees of partial melting of a peridotitic source representative of the convecting normal MORB mantle. Fractional crystallization of olivine, clinopyroxene, and amphibole (i.e. the dominant phases observed in Santa Rosa sills and lava flow) cannot increase significantly K_2O/Na_2O ratio in the residual melt as demonstrated by the liquid line of descent determined experimentally at 1.5 GPa for an initial basanitic liquid [*Pilet et al.*, 2010]. The study of *Pilet et al.* [2010] shows that K_2O/Na_2O remains mostly constant for melts evolving during fractional crystallisation of, first, an olivine + clinopyroxene assemblage, then an amphibole + clinopyroxene assemblage. Partial melting curves calculated assuming primitive mantle source composition indicates that the K_2O content of these basalts can form by very low degrees of partial melting (<1 %) (Figure 4d), but *Prytulak and Elliot* [2007] showed that the source of Ti-rich rocks needs to be more enriched than the primitive mantle to satisfy the TiO_2 content of the basalts. In addition, the Al_2O_3 content at given MgO content observed in Santa Rosa and petit-spot lavas (Figure 4b) is significantly lower than that produced during partial melting experiments performed between 2.5 and 4 GPa from fertile peridotite [*Hirose and Kushiro*, 1993; *Kushiro*, 1996; *Walter*, 1998; Davis *et al.*, 2011]. *Machida et al.* [2009] propose that source enrichment including K, Rb, Ba of petit-spot volcanoes reflects melting of recycled material in an asthenospheric magma source. Nevertheless, it is not clear if melting of this assemblage can satisfactorily lead to the observed Al_2O_3 content. We propose here an alternate model that accounts for the major and trace element contents of the potassic alkaline basalts through a two-step process:

(1) Peridotite melts are continuously extracted from the low-velocity zone at the base of the oceanic lithosphere (in the stability field of garnet) and percolate through the lower lithosphere producing metasomatic phlogopite-pyroxenite veins at depth [*Lloyd et al.*, 1975; *Harte et al.*, 1993; *Niu and O'Hara*, 2003];

(2) Tectonic stress triggering lithosphere cracking allows melts from the low-velocity zone to interact with the phlogopite-pyroxenite veins, re-melt them and mix before reaching the surface to produce potassic lavas. The tectonic stress may be related to plate flexure as in the case of petit-spot volcanoes in Japan or by diffuse lithospheric extension as proposed for seamounts observed in the Line Islands chain.

Phlogopite is characterized by high K_2O and TiO_2 content and incorporates Ba and Rb preferentially with respect to Th, U or REE. The presence of this mineral in the source of potassic lavas has long been postulated in continental settings [*Lloyd et al.*, 1975; *Edgar*, 1987; *Foley*, 1992]. The presence of amphibole in the source of alkaline rocks has been also proposed to explain K anomalies in alkaline basalts. Nevertheless, amphiboles observed in metasomatized peridotite or in metasomatic veins are characterized by K_2O/Na_2O ratio < 1 [*Pilet et al.*, 2008], which is inconsistent with the formation of K-rich basalt via incongruent melting of amphibole-bearing peridotite or metasomatic veins. Phlogopite, on the other hand, can successfully explain unusual K, Ti, Ba and Rb contents as well as K_2O/Na_2O ratios observed in potassic alkaline basalts in the ocean (Figures 4 and 8). Because phlogopite is not stable above ~1200°C, which is the approximate temperature at the base of the lithosphere [*Konzett and Ulmer*, 1999], the occurrence of this mineral restricts its origin to parts of the lithosphere rather than in the convecting mantle where temperatures exceed 1200°C. Also, our model is supported by the compositional range of major elements of the studied basalts, which define a mixing line between low degrees of peridotite melting and experimental melts from metasomatic phlogopite-clinopyroxene veins [*Lloyd et al.*, 1985] (Figure 4). As

indicated previously, the Al_2O_3 content of the Santa Rosa and Japanese petit-spot basalts is significantly lower than that observed in experimental partial melts from peridotitic sources, hence requiring an additional (e.g. metasomatic) component in the source.

5.3. Formation of the seamount by lithosphere cracking

The wide range of observations above outlines very consistently the occurrence of an accreted small-sized seamount volcanologically and compositionally similar to petit-spot volcanoes in Japan. However, lithological and age constraints indicate that the accreted edifice is unlikely to have formed close to a subduction zone. Petrological and seismic data show that melt may be ubiquitous at the base of the oceanic lithosphere [*Kawakatsu et al.*, 2009; *Ni et al.*, 2011]. This melt could be collected through lithospheric fractures over large areas and trigger low-volume volcanism without need for decompression, convection or thermal anomalies in the mantle [*Natland and Winterer*, 2005; *Presnall and Gudfinnsson*, 2011]. Potassic alkaline basalts such as those forming the Santa Rosa seamount or petit-spot volcanoes in Japan have been rarely sampled compared to other OIBs. This may be related to the difficulty in sampling low volumes of potassic alkaline basalts in the ocean, but the occurrence of petit-spot-like volcanoes could be much larger than commonly assumed. Interestingly, potassic alkaline basalts have also been reported from the top or flank of larger volcanic edifices of the Line Islands chain and Wake seamounts [*Natland*, 1976; *Davis et al.*, 2002]. Volcanism at the Line Islands chain has no age progression and occurred during several periods over a widespread area [*Davis et al.*, 2002]. Hence, similarly to the formation of petit-spot volcanoes due to slab flexure in Japan [*Valentine and Hirano*, 2010], the formation of the chain is considered to be related to lithosphere cracking rather than persistent melting anomalies [*Davis et al.*, 2002; *Natland and Winterer*, 2005]. Our data cannot rule out the possibility that the studied seamount formed in response to thermal anomalies in the mantle. However, the unusual composition of the Santa Rosa basalts and their similarity to

petit-spot and Line Islands lavas suggest that they formed in response to similar processes of lithosphere cracking. This interpretation is in good agreement with petrological constraints showing that potassic alkaline basalts can form in response to mixing of low degree partial melts of a garnet peridotite in the upper asthenosphere with metasomatic veins at the base of the lithosphere (i.e. a process viable in the ocean without abnormally-high thermal gradients in the uppermost mantle).

Placing the Early/Middle Jurassic accreted seamount of Santa Rosa in its original context of formation is limited by poor preservation of Jurassic ocean crust and difficulties in reconstructing tectonic development of the Pacific basin in the early Mesozoic. Clues about this development come from circum-Pacific terranes and tomographic anomalies in the sub-Pacific mantle, which indicate that several volcanic arcs transited across the basin and, notably, accreted on its western side [*Nokleberg et al.*, 2000; *Smith*, 2007; *Bandini et al.*, 2011b; *van der Meer*, 2012]. Upper Paleozoic seamounts are preserved in the Canadian cordillera, which accreted at ~230 Ma along an intra-oceanic volcanic arc and were subsequently emplaced along North America during arc-continent collision at ~180 Ma [*Johnston and Borel*, 2007]. Tethyan fauna associated with the seamounts show that these volcanic edifices were able to cross over the entire Panthalassa, with successive emplacements along intra-oceanic and continental convergent plate boundaries (i.e., seamount accretion and arc-continent collision). In this context it remains unclear where the Santa Rosa seamount accreted and how it was driven to its present location. However, our data clearly show that its formation was distant from volcanic arcs and mid-ocean ridges. In addition, formation of the seamount at ~175 Ma is coeval with major plate reorganization in the Pacific basin. *Bartolini and Larson* [2001] estimated that formation of the Pacific plate related to break-up of the Izanagi, Farallon and Phenix plates initiated at 175-170 Ma. They proposed that this plate re-organisation was triggered by the break-up of Pangea, opening of the

Atlantic, and increased subduction rates on the western side of the Pacific basin. Changes of subduction patterns have also been proposed by *Natland and Winterer* [2005] to exert a strong control on plate tectonics, which may have notably allowed lithosphere cracking and formation of some of the linear volcanic chains seen in the recent Pacific basin. In an alternative interpretation, incipient formation of the Pacific plate during the Middle/Late Jurassic was primarily caused by deep-seated, mantle processes [*Pavoni*, 2003]. In any case, it is clear that significant re-distribution of stress in the lithosphere accompanied the break-up of the Izanagi, Farallon and Phoenix plates. We hypothesize therefore that this event was associated with lithosphere cracking across the now-disappeared Farallon Plate, which led to low-volume intraplate volcanism and formation of the studied seamount.

6. Summary and conclusions

The Santa Rosa Accretionary Complex includes a small-sized seamount formed in the Middle/Late Jurassic (~175 Ma) on a now-disappeared plate segment of the Pacific basin, which accreted in the Early Cretaceous (~110 Ma) along an unknown convergent plate boundary. Potassic alkaline basalts found in the seamount are very uncommon in the ocean and have previously been reported from petit-spot volcanoes off Japan, surficial deposits on seamounts of the Line Islands chain and one occurrence at the Wake seamounts. In Japan and along the Line Islands chain, emplacement of the basalts is clearly associated with lithosphere cracking. Similarly, petrogenetic constraints show that the Santa Rosa potassic alkaline basalts (and similar rocks in the ocean) can form by percolation of melts pre-existing at the base of the lithosphere in the low-velocity zone. These melts interact on their way to the surface with metasomatic veins previously formed in the lower lithosphere, and allow formation of small-sized seamounts or emplacement of small volumes of lavas/sills on larger seamounts. The Santa Rosa seamount closely resembles petit-spot volcanoes in Japan, but its formation in an intraplate setting suggests that small-sized seamounts similar to petit-spot

volcanoes can also occur disconnected from subduction zones. Petrological and contextual constraints on the origin of potassic alkaline basalts combined with formation of the Santa Rosa seamount coeval with incipient formation of the Pacific plate at ~175-170 Ma suggest that the formation of the seamount occurred in response to lithosphere cracking during major re-organisation of plate tectonics in the Pacific basin. Growing number of potassic alkaline basalts observed in seamount settings suggests that they may represent a common, yet poorly known expression of low-volume intraplate volcanism in the ocean.

Acknowledgements

We thank Godfrey Fitton, Anthony Koppers, James Natland and an anonymous reviewer for their insightful and constructive review. We thank Peter Ulmer for sharing unpublished experimental data on amphibole crystallization. People from the Santa Rosa National Park provided support during field work. Discussions with Kaj Hoernle, Folkmar Hauff and Maxim Portnyagin helped preparing the manuscript. This paper was conceived and written during the tenure of a postdoctoral fellowship at the IFM-GEOMAR (SNSF Grant #PA00P2-134128/1).

REFERENCES CITED

Bandini, A. N., P. O. Baumgartner, K. Flores, P. Dumitrica, and S.-J. Jackett (2011a), Early Jurassic to early Late Cretaceous radiolarians from the Santa Rosa accretionary complex (northwestern Costa Rica), *Ofioliti*, *36*(1), 1-35.

Bandini, A. N., P. O. Baumgartner, K. Flores, P. Dumitrica, C. Hochard, G. M. Stampfli, and S.-J. Jackett (2011b), Aalenian to Cenomanian Radiolaria of the Bermeja Complex (Puerto Rico) and Pacific origin of radiolarites on the Caribbean Plate, *Swiss Journal of Geosciences*, *104*(3), 367-408.

Bartolini, A., and R. L. Larson (2001), Pacific microplate and the Pangea supercontinent in the Early to Middle Jurassic, *Geology*, *29*(8), 735-738.

Baumgartner, P. O., and P. Denyer (2006), Evidence for middle Cretaceous accretion at Santa Elena

Peninsula (Santa Rosa Accretionary Complex), Costa Rica, *Geologica Acta*, *4*(1-2), 179-191.

Buchs, D. M., R. J. Arculus, P. O. Baumgartner, C. Baumgartner-Mora, and A. Ulianov (2010), Late Cretaceous arc development on the SW margin of the Caribbean Plate: Insights from the Golfito, Costa Rica, and Azuero, Panama, complexes, *Geochemistry Geophysics Geosystems*, *11*(7), Q07S24.

Buchs, D. M., R. J. Arculus, P. O. Baumgartner, and A. Ulianov (2011), Oceanic intraplate volcanoes exposed: Example from seamounts accreted in Panama, *Geology*, *39*(4), 335-338.

Davis, A. S., L. B. Gray, D. A. Clague, and J. R. Hein (2002), The Line Islands revisited: New 40Ar/39Ar geochronologic evidence for episodes of volcanism due to lithospheric extension, *Geochemistry Geophysics Geosystems*, *3*(3), 1018.

Davis, F. A., Hirschmann, M. M., Humayun, M. (2011) The composition of the incipient partial melt of garnet peridotite at 3 GPa and the origin of OIB, *Earth and Planetary Science Letters*, *308*(3-4), 380-390.

Edgar, A. D. (1987), The genesis of alkaline magmas with emphasis on their source regions: inferences from experimental studies, in *Alkaline Igneous Rocks*, edited by J. G. Fitton and B. G. J. Upton, Geological Society, London, Special Publication, *33*, 29-52.

Foley, S. (1992), Vein-plus-wall-rock melting mechanisms in the lithosphere and the origin of potassic alkaline magmas, *Lithos*, *28*(3-6), 435-453.

Fujiwara, T., N. Hirano, N. Abe, and K. Takizawa (2007), Subsurface structure of the "petit-spot" volcanoes on the northwestern Pacific Plate, *Geophysical Research Letters*, *34*(13), L13305.

Geldmacher, J., K. Hoernle, P. van den Bogaard, F. Hauff, and A. Klügel (2008), Age and geochemistry of the Central American forearc basement (DSDP Leg 67 and 84): Insights into Mesozoic arc volcanism and seamount accretion, *Journal of Petrology*, *49*(10), 1781-1815.

Harte, B., R. H. Hunter, and P. D. Kinny (1993), Melt Geometry, Movement and Crystallization, in Relation to Mantle Dykes, Veins and Metasomatism, *Philosophical Transactions of the Royal Society of London. Series A: Physical and Engineering Sciences*, *342*(1663), 1-21.

Hauff, F., K. A. Hoernle, P. van den Bogaard, G. E. Alvarado, and D. Garbe-Schonberg (2000), Age and geochemistry of basaltic complexes in Western Costa Rica: Contributions

to the geotectonic evolution of Central America, *Geochemistry Geophysics Geosystems*, *1*(5), 1009, doi:1010.1029/1999GC000020.

Hillier, J. K., and A. B. Watts (2007), Global distribution of seamounts from ship-track bathymetry data, *Geophysical Research Letters*, *34*, L13304.

Hirano, N., et al. (2006), Volcanism in response to plate flexure, *Science*, *313*(5792), 1426-1428.

Hirano, N., A. A. P. Koppers, A. Takahashi, T. Fujiwara, and M. Nakanishi (2008), Seamounts, knolls and petit-spot monogenetic volcanoes on the subducting Pacific Plate, *Basin Research*, *20*(4), 543-553.

Hirose, K., and I. Kushiro (1993), Partial melting of dry peridotites at high pressures: Determination of compositions of melts segregated from peridotite using aggregates of diamond, *Earth and Planetary Science Letters*, *114*(4), 477-489.

Hoernle, K., P. van den Bogaard, R. Werner, B. Lissinna, F. Hauff, G. Alvarado, and D. Garbe-Schonberg (2002), Missing history (16-71 Ma) of the Galpapagos hotspot: Implications for the tectonic and biological evolution of the Americas, *Geology*, *30*(9), 795-798.

Johnston, S. T., and G. D. Borel (2007), The odyssey of the Cache Creek terrane, Canadian Cordillera: Implications for accretionary orogens, tectonic setting of Panthalassa, the Pacific superwell, and break-up of Pangea, *Earth and Planetary Science Letters*, *253*(3-4), 415-428.

Kägi, R. (2000), *The Liquid Line of Descent of Hydrous, Primary, Calcalkaline Magmas Under Elevated Pressure. An Experimental Approach.*, PhD Thesis, 115 p., ETH Zürich.

Kawakatsu, H., P. Kumar, Y. Takei, M. Shinohara, T. Kanazawa, E. Araki, and K. Suyehiro (2009), Seismic Evidence for Sharp Lithosphere-Asthenosphere Boundaries of Oceanic Plates, *Science*, *324*(5926), 499-502.

Kimura, G., and J. Ludden (1995), Peeling Oceanic-Crust in Subduction Zones, *Geology*, *23*(3), 217-220.

Konzett, J., and P. Ulmer (1999), The Stability of Hydrous Potassic Phases in Lherzolitic Mantle: an Experimental Study to 9.5 GPa in Simplified and Natural Bulk Compositions, *Journal of Petrology*, *40*(4), 629-652.

Kushiro, I. (1996), Partial melting of a fertile mantle peridotite at high pressures: an

experimental study using aggregates of diamond, in *Earth Processes: Reading the Isotopic Code*, edited by A. Basu and S. Hart, pp. 109-122, Washington, DC.

Legendre, C., et al. (2005), Origin of Exceptionally Abundant Phonolites on Ua Pou Island (Marquesas, French Polynesia): Partial Melting of Basanites Followed by Crustal Contamination, *Journal of Petrology*, *46*(9), 1925-1962.

Lloyd, F. E., and D. K. Bailey (1975), Light element metasomatism of the continental mantle: The evidence and the consequences, *Physics and Chemistry of The Earth*, *9*(0), 389-416.

Lloyd, F. E., M. Arima, and A. D. Edgar (1985), Partial melting of a phlogopite-clinopyroxenite nodule from south-west Uganda: an experimental study bearing on the origin of highly potassic continental rift volcanics, *Contributions to Mineralogy and Petrology*, *91*(4), 321-329.

Machida, S., N. Hirano, and J.-I. Kimura (2009), Evidence for recycled plate material in Pacific upper mantle unrelated to plumes, *Geochimica et Cosmochimica Acta*, *73*(10), 3028-3037.

Matsuda, S., and Y. Ogawa (1993), Two-stage model of incorporation of seamount and oceanic blocks into sedimentary melange: Geochemical and biostratigraphic constraints in Jurassic Chichibu accretionary complex, Shikoku, Japan, *The Island Arc*, *2*, 7-14.

McDonough, W. F., and S. S. Sun (1995), The Composition of the Earth, *Chemical Geology*, *120*(3-4), 223-253.

Meschede, M., and W. Frisch (1994), Geochemical characteristics of basaltic rocks from the Central American ophiolites, *Profil*, *7*, 71-85.

Natland, J. H. (1976), Petrology of volcanic rocks dredged from seamounts in the Line Islands, in *Initial Reports of the Deep Sea Drilling Project*, p. 749-777, Texas A & M University, Ocean Drilling Program, College Station, TX, United States.

Natland, J. H., and E. L. Winterer (2005), Fissure control on volcanic action in the Pacific, in *Plates, plumes and paradigms*, edited by G. R. Foulger, J. H. Natland, D. C. Presnall and D. L. Anderson, pp. 687-710.

Nekvasil, H., A. Dondolini, J. Horn, J. Filiberto, H. Long, and D. H. Lindsley (2004), The Origin and Evolution of Silica-saturated Alkalic Suites: an Experimental Study, *Journal of Petrology*, *45*(4), 693-721.

Ni, H., H. Keppler, and H. Behrens (2011), Electrical conductivity of hydrous basaltic melts: implications for partial melting in the upper mantle, *Contributions to Mineralogy and Petrology*, *162*(3), 637-650.

Niu, Y., and R. Batiza (1997), Trace element evidence from seamounts for recycled oceanic crust in the Eastern Pacific mantle, *Earth and Planetary Science Letters*, *148*(3-4), 471-483.

Niu, Y., and M. J. O'Hara (2003), Origin of ocean island basalts: A new perspective from petrology, geochemistry, and mineral physics considerations, *J. Geophys. Res.*, *108*(B4), 2209.

Nokleberg, W. J., L. M. Parfenov, J. W. H. Monger, I. O. Norton, A. I. Khanchuk, D. B. Stone, C. R. Scotese, D. W. Scholl, and K. Fujita (2000), Phanerozoic Tectonic Evolution of the Circum-North Pacific, *U.S. Geological Survey Professional Paper*, *1626*, 1-122.

Okamura, Y. (1991), Large-scale melange formation due to seamount subduction: an example from the Mesozoic accretionary complex in central Japan, *Journal of Geology*, *99*(5), 661-674.

Pavoni, N. (2003), Pacific microplate and the Pangea supercontinent in the Early to Middle Jurassic: Comment and Reply, *Geology*, *31*(1), e1-e2.

Pilet, S. b., M. B. Baker, and E. M. Stolper (2008), Metasomatized Lithosphere and the Origin of Alkaline Lavas, *Science*, *320*(5878), 916-919.

Pilet, S., P. Ulmer, and S. Villiger (2010), Liquid line of descent of a basanitic liquid at 1.5 Gpa: constraints on the formation of metasomatic veins, *Contributions to Mineralogy and Petrology*, *159*(5), 621-643.

Presnall, D. C., and G. H. Gudfinnsson (2011), Oceanic Volcanism from the Low-velocity Zone - without Mantle Plumes, *Journal of Petrology*.

Prytulak, J., and T. Elliott (2007), TiO2 enrichment in ocean island basalts, *Earth and Planetary Science Letters*, *263*(3-4), 388-403.

Reynolds, J. R., and C. H. Langmuir (2000), Identification and implications of off-axis lava flows around the East Pacific Rise, *Geochemistry Geophysics Geosystems*, *1*(6), 1-25.

Smith, A. D. (2007), A plate model for Jurassic to Recent intraplate volcanism in the Pacific Ocean basin, in *Plates, Plumes and Planetary Processes*, edited by G. R. Foulger and D. M. Jurdy, pp. 471-495.

Tiepolo and, M., R. Vannucci, P. Bottazzi, R. Oberti and, A. Zanetti, and S. Foley (2000), Partitioning of rare earth elements, Y, Th, U, and Pb between pargasite, kaersutite, and basanite to trachyte melts: Implications for percolated and veined mantle, *Geochem. Geophys. Geosyst.*, *1*(8).

Tournon, J. (1994), The Santa Elena Peninsula: an ophiolitic nappe and a sedimentary volcanic relative autochtonous, *Profil*, *7*, 87-96.

Valentine, G. A., and N. Hirano (2010), Mechanisms of low-flux intraplate volcanic fields - Basin and Range (North America) and northwest Pacific Ocean, *Geology*, *38*(1), 55-58.

van der Meer, D. G., T. H. Torsvik, W. Spakman, D. J. J. van Hinsbergen, and M. L. Amaru (2012), Intra-Panthalassa Ocean subduction zones revealed by fossil arcs and mantle structure, *Nature Geosci*, *5*(3), 215-219.

Walter, M. J. (1998), Melting of Garnet Peridotite and the Origin of Komatiite and Depleted Lithosphere, *Journal of Petrology*, *39*(1), 29-60.

Wessel, P., D. T. Sandwell, and S.-S. Kim (2010), The Global Seamount Census, *Oceanography*, *23*(1), 24-33.

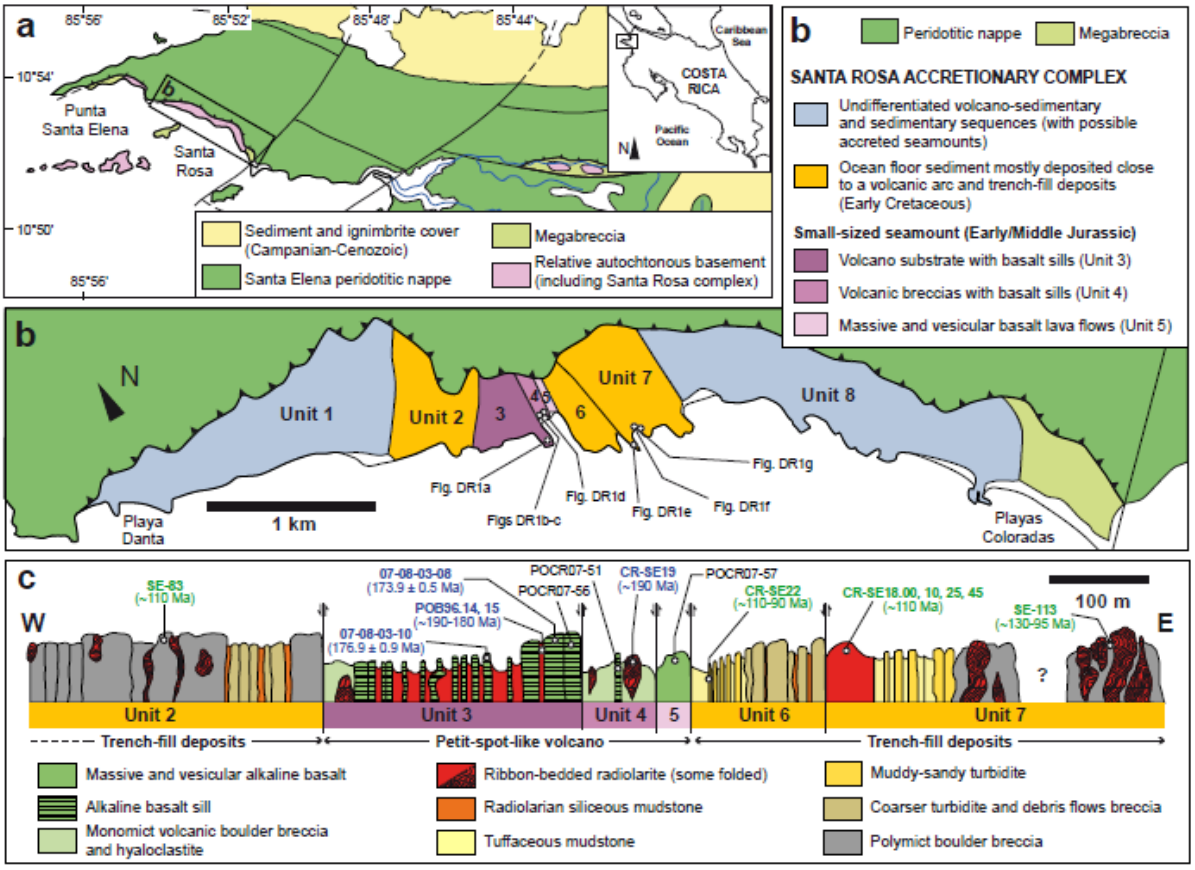

Figure 1. Geological framework of the Santa Rosa accretionary complex. (a) Geological map of the Santa Elena peninsula. (b) Geological sketch map of the Santa Rosa accretionary complex with location of pictures shown in Figure 2. (c) Idealized cross-section showing studied lithologic assemblages, with location of analyzed basalts and samples that constrain the age of formation of the units (blue = Middle/Late Jurassic, green = Early Cretaceous, black = undefined formation age).

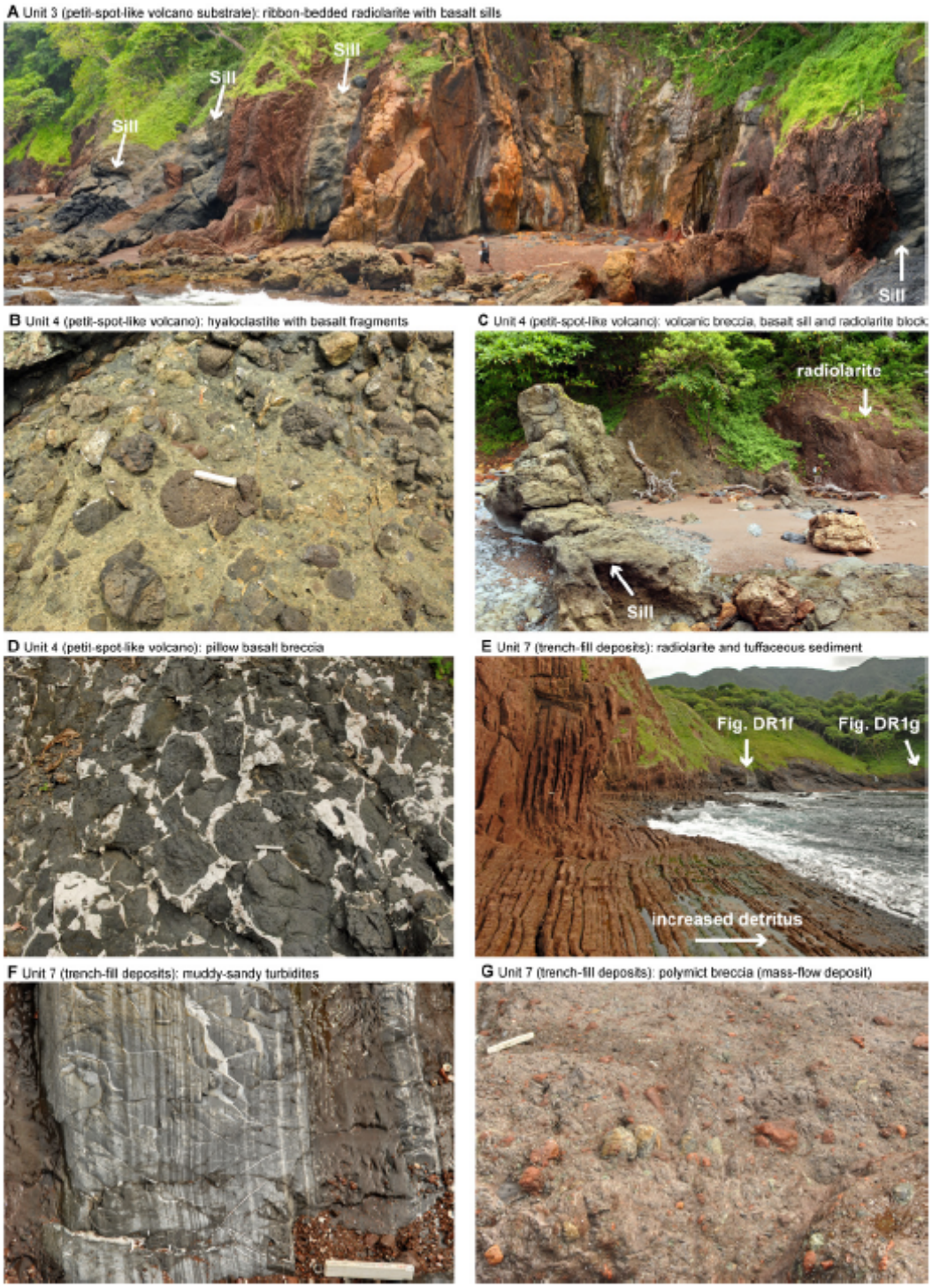

Figure 2. Lithologic assemblages of the Santa Rosa Accretionary Complex (locations on Figure 1b). (a-d) petit-spot volcano sequences. (e-f) trench-fill deposits.

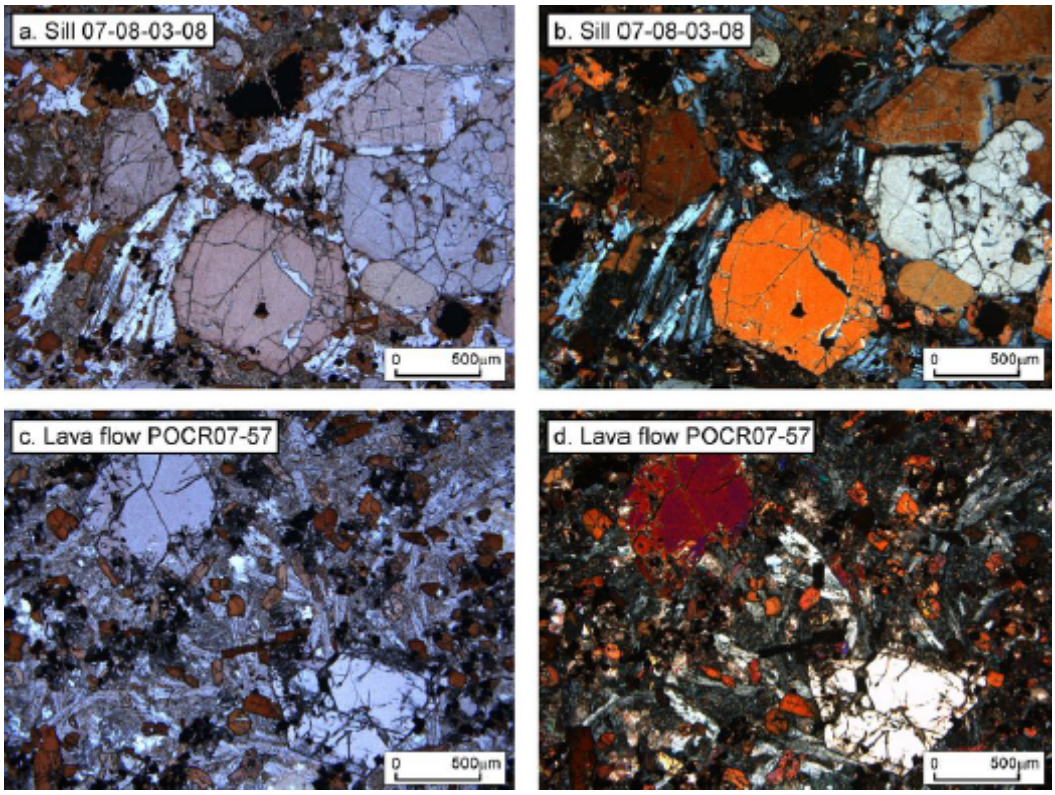

Figure 3. Photomicrographs of a Santa Rosa sill (07-08-03-08) and lava flow (POCR-07-57). (a, c) plane polarized light. (b, d) with crossed polars. (a-d) Note the porphyric texture of Santa Rosa basalts and the different degrees of alteration in the matrix. These rocks are characterized by large phenocrysts of augite (500-2000 µm in size) associated with amphibole and Fe-Ti oxides micro-phenocrysts (500- 50 µm in size), which are embedded in a finer-grained matrix of plagioclase, augite, amphibole, Fe-Ti oxides, apatite and glass. The phenocrysts and microphenocrysts are unaltered, but the glass show evidence of palagonitization. The main differences between the two displayed samples are the degree of alteration of the plagioclase in the matrix and larger amounts of cumulative augite in the sill.

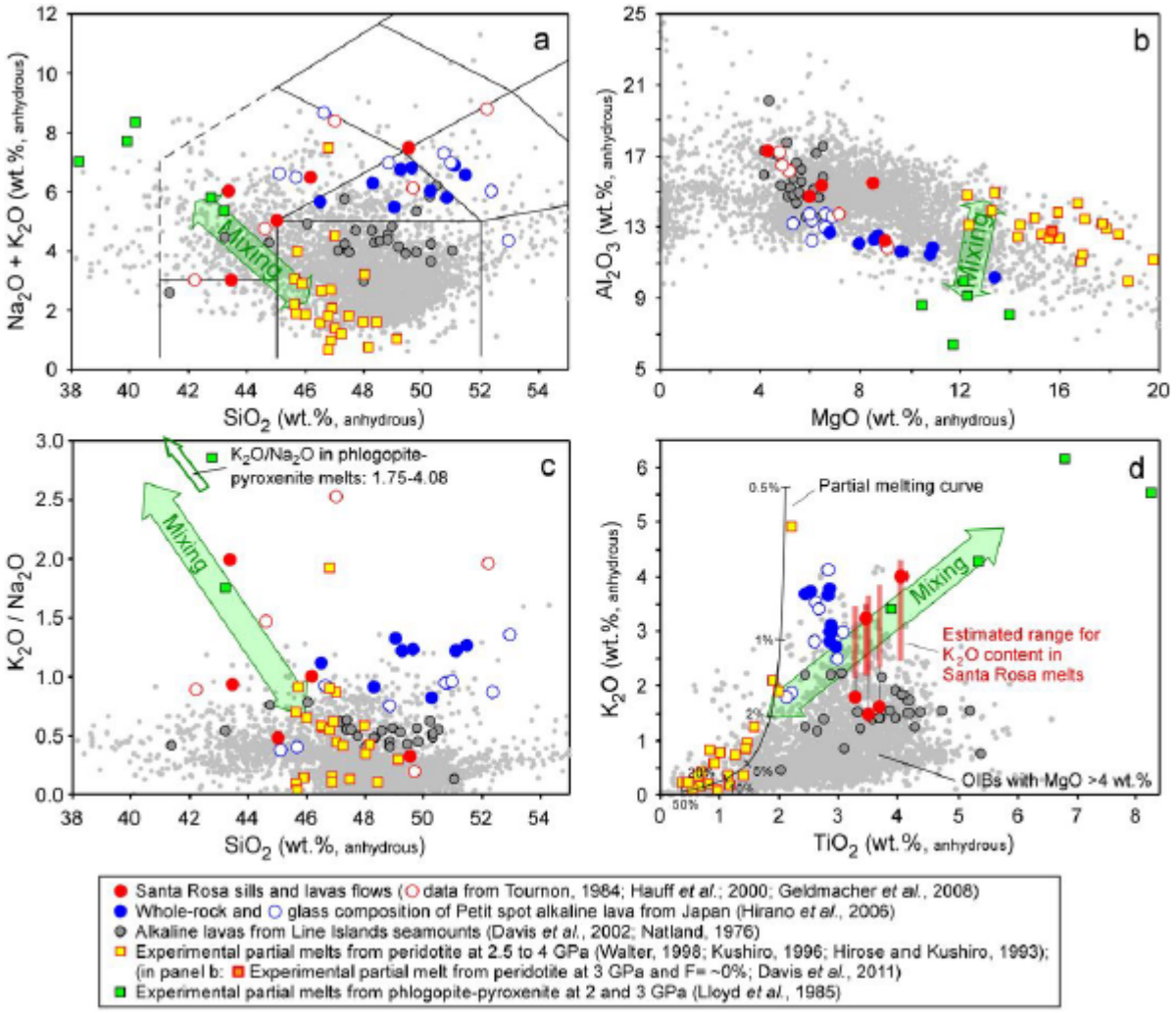

Figure 4. Major oxides content and ratio for Santa Rosa sills and associated lava flows compared to ocean island basalts (OIBs, GeoRoc database) and experimental melts from peridotite produced at pressure between 2.5 and 4 GPa [*Hirose and Kushiro*, 1993; *Kushiro*, 1996; *Walter*, 1998; *Davis et al.*, 2011], and from phlogopite-clinopyroxenite at 2 and 3 GPa [*Lloyd et al.*, 1985]. (a) SiO_2 vs $Na_2O + K_2O$. (b) MgO vs Al_2O_3. (c) SiO_2 vs K_2O/Na_2O. (d) TiO_2 vs K_2O. (a-d) the green arrow represents potential mixing between melts from peridotite and phlogopite clinopyroxenite. see the main text for the detail of calculation of the K contents in equilibrium with amphibole phenocrysts from Santa Rosa lava reported in panel (d), and Supplemental Data for the detail of calculation related to the batch melting curve for K_2O and TiO_2. Data from *Davis et al.* (2011) are reported only in panel b regarding that K content in their experiments are fixed to 1 wt. %.

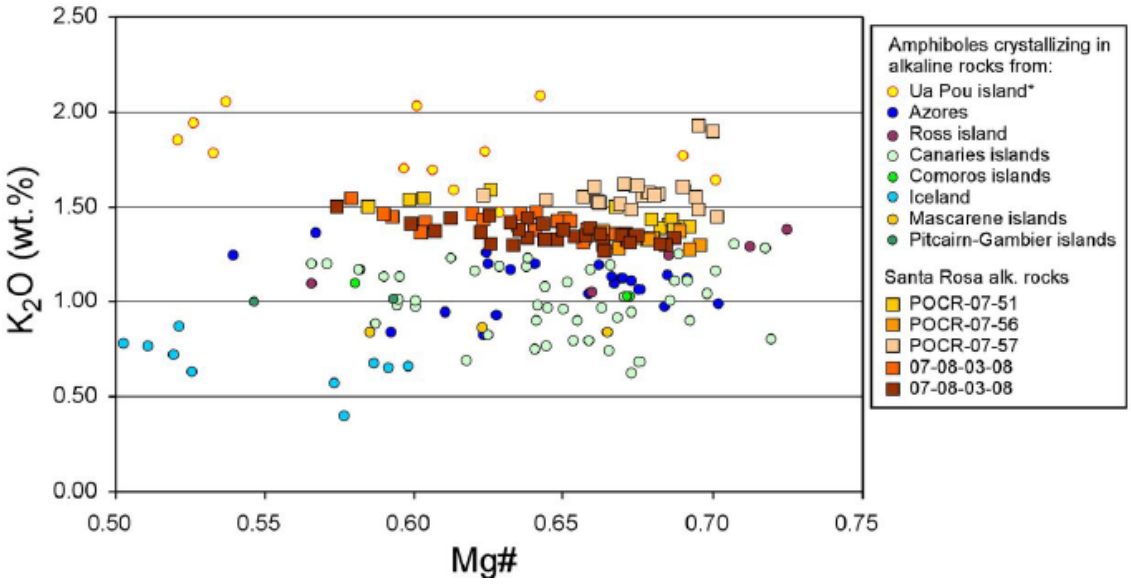

Figure 5. Mg# versus K_2O content in amphibole phenocrysts from Santa Rosa alkaline rocks compared with amphibole phenocrysts crystallizing in alkaline rocks from various oceanic islands. The amphiboles from Santa Rosa lavas and sills show higher K_2O for a given Mg# than the amphiboles from typical oceanic alkaline series suggesting crystallisation in a slightly more K-rich liquid than observed in typical oceanic islands. Sole exception consists of amphiboles from Ua Pou Island (Marquesas, French Polynesia), which show slightly higher K content than those observed in amphiboles from Santa Rosa. Nevertheless, the Uo Pou tephri-phonolites and phonolites from which the amphiboles have crystallized are rich in K (K_2O > 5 wt.%) with K2O/Na2O ratios close to 1. In addition, the formation of these rocks is not interpreted as resulting from fractional crystallization of a primary alkaline basaltic liquid but reflects the partial melting at depth of basanites [*Legendre et al.*, 2005]. Amphibole data from oceanic islands are selected from the GeoRoc database.

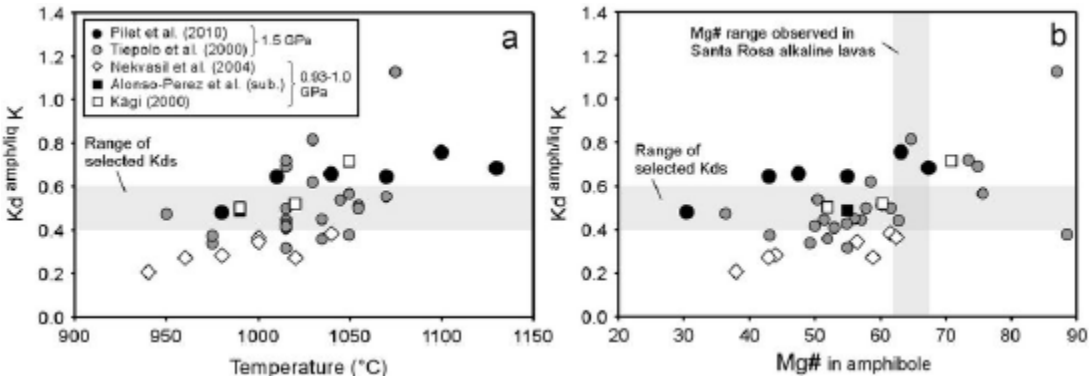

Figure 6. Variation of Kd $^{amphibole/liq}$ for K_2O versus (a) experimental temperature and (b) Mg# in amphibole in various fractional (FC) and equilibrium crystallization experiments. Data points represent: FC experiments of an initial nepheline-normative basanite at 1.5 GPa (filled black circles; *Pilet et al.* [2010]); a hypersthene-normative hawaiite at 0.93 GPa (open black diamonds; *Nekvasil et al.* [2004]), and a hypersthene-normative picrobasalt at 1.5 GPa (filled black squares; *Alonso-Perez et al.* submitted) and 1.0 GPa (open black squares; *Kägi* [2000]). Amphiboles from equilibrium crystallization experiments are taken from *Tiepolo et al.* [2000] at 1.5 GPa (filled grey circles) and are shown for comparison.

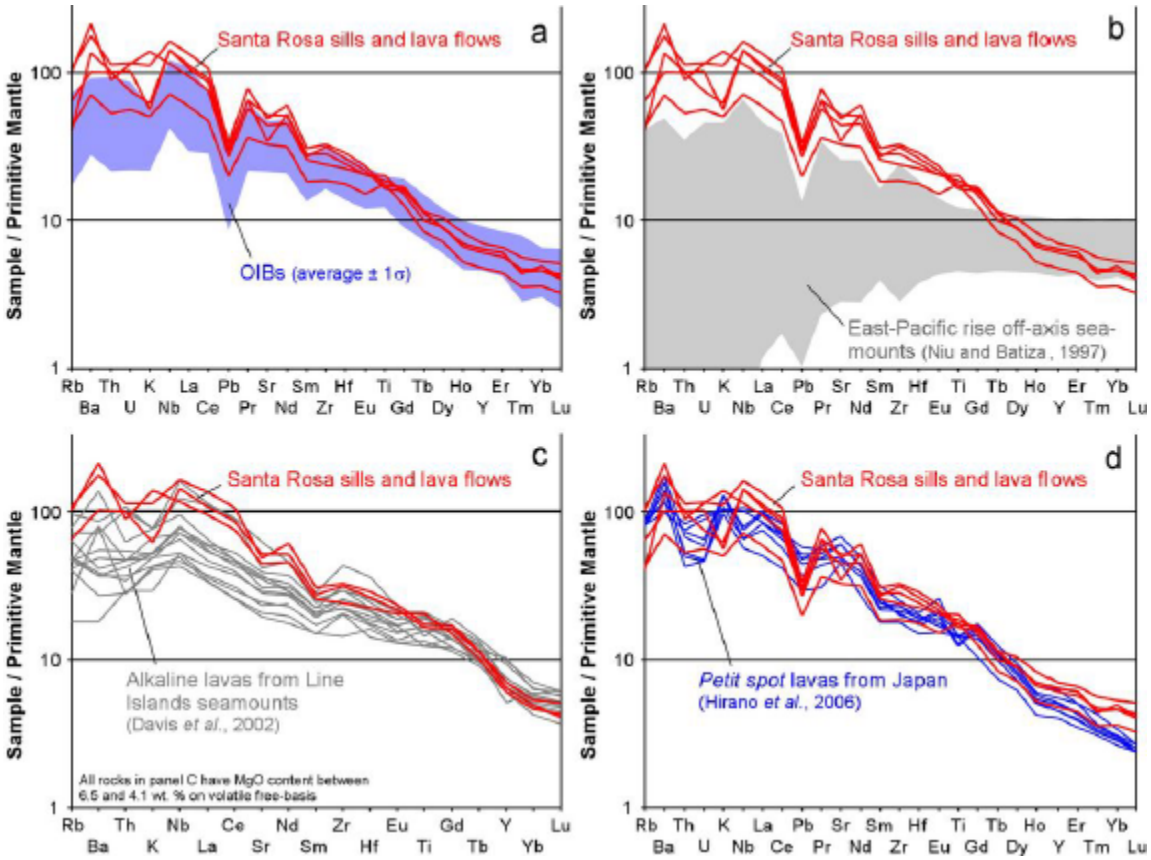

Figure 7. Variation of K_2O content in amphiboles as function of crystallization temperature and pressure observed in equilibrium experiments from an initial basanitic liquid [*Peter Ulmer*, unpublished data]. 0.2 – 0.4 GPa experiments have been performed in an internally heated pressure vessel (Clermont- Ferrand) using Ag75Pd25 capsules providing a $fO_2 \geq$ NNO. The 0.5 – 3.0 GPa Piston-cylinder experiments have been performed at ETH Zurich using graphite-Pt double capsules ($fO_2 \approx$ FMQ -1 to -3). The composition of the nepheline normative hydrous-basanitic starting material is typical of basanite observed in oceanic or continental setting with a K_2O content of 0.93 wt. %.

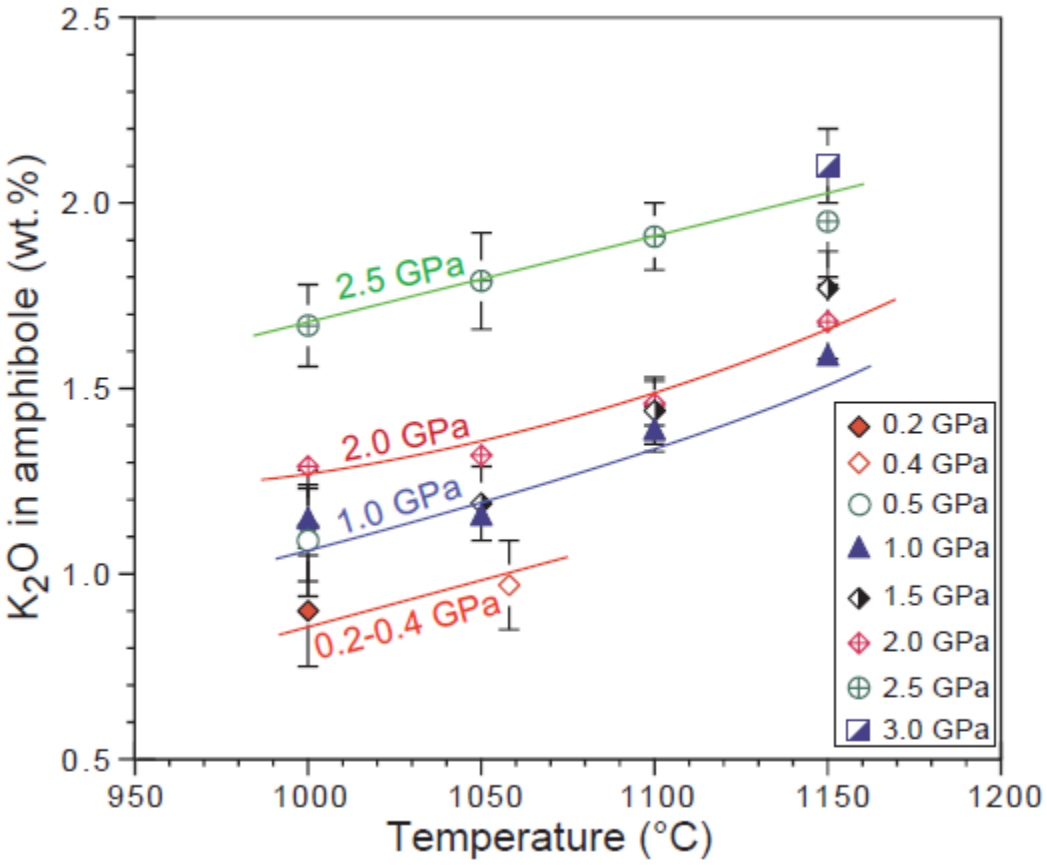

Figure 8. PM-normalized trace element patterns of Santa Rosa basalts. (a) Comparison with ocean island basalts (OIBs, GeoRoc database, 752 samples with SiO_2=42-48 wt % and MgO=6-5 wt %). (b) Comparison with East Pacific Rise off-axis seamounts [*Niu and Batiza*, 1997]. (c) Comparison with Line Islands seamounts [*Davis et al.*, 2002]. Only the Line Islands rocks characterized by LOI below 4 wt.%, MgO content between 4 and 6.5 wt. %, and P_2O_5 content lower that 2 wt. % are reported. Only Santa Rosa sills with MgO content between 4 and 6.5 wt. % are shown for comparison. (d) Comparison with petit-spot lavas from Japan [*Hirano et al.*, 2006].

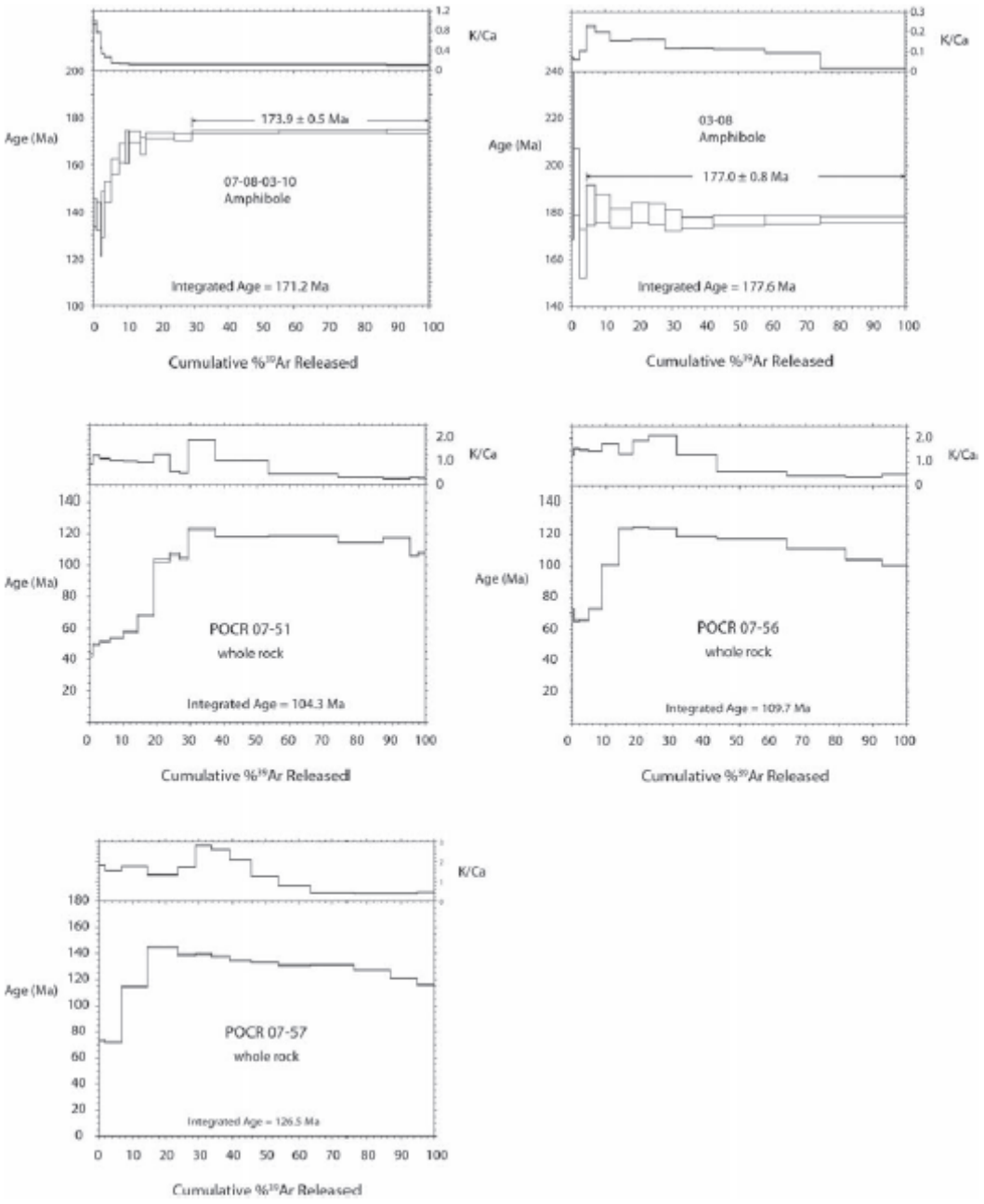

Figure 9. ^{40}Ar-^{39}Ar step-heating diagrams. Complete data are given in Table S3.

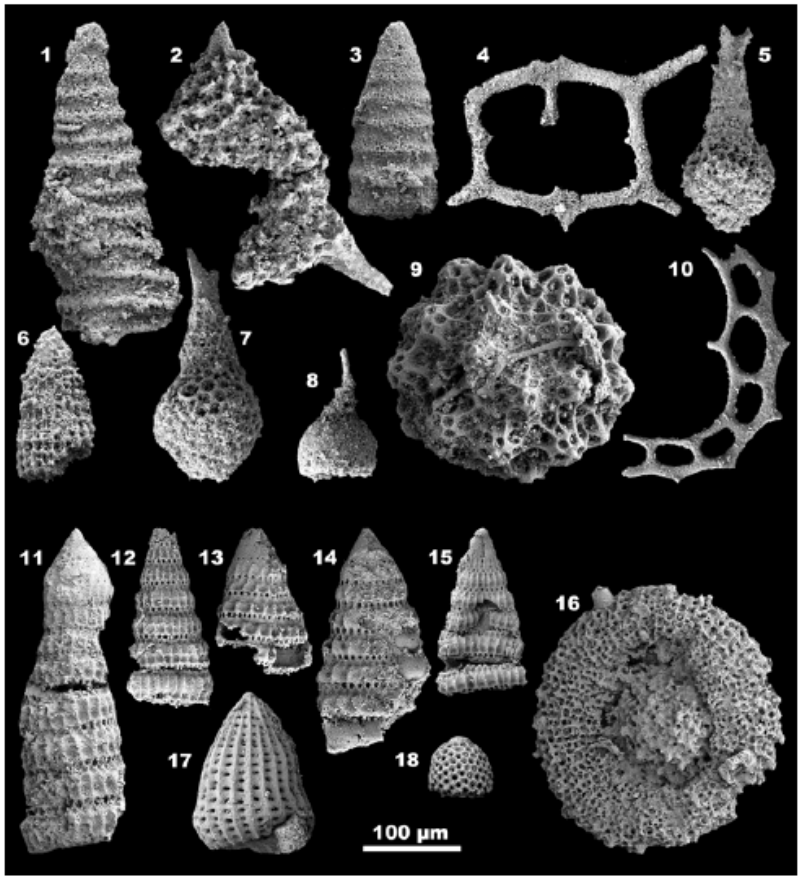

Figure 10. Late Early Jurassic and late Early Cretaceous Radiolaria (biochronologic range of each species indicated where known) from the Santa Rosa Accretionary Complex. 1-5) Sample CR-SE19, early-middle Pliensbachian, from a radiolarite block in unit 4. 1) *Canoptum columbiaense* WHALEN and CARTER (latest Sinemurian – Pliensbachian) . 2) *Cyclastrum* asuncionense WHALEN and CARTER (early-middle Pliensbachian). 3) *Canoptum dixoni* PESSAGNO and WHALEN (latest Sinemurian – Pliensbachian). 4) *Paleosaturnalis tetraradiatus* KOZUR and MOSTLER (latest Sinemurian – middle Pliensbachian). Sample POB96-14. 5) Katroma bicornis DE WEVER (Pliensbachian-early Toarcian). 6-10) Samples POB96-15, early Toarcian, from ribbon cherts interbedded with alkaline basalt sills of unit 3. 6) *Parahsuum ovale* HORI and YAO (latest Sinemurian – Toarcian). 7) Katroma bicornis DE WEVER (Pliensbachian – early Toarcian). 8) *Eucyrtidiellum disparile* gr. NAGAI and MIZUTANI (Toarcian – Bajocian). 9) *Praeconocaryomma bajaensis* WHALEN (Pliensbachian – Aalenian). 10) *Parasaturnalis diplocyclis* (YAO) (Pliensbachian – early Bajocian). 11-19) Early-middle Albian samples from continuous radiolarite-trench fill section in unit 7. 11-12) Sample CRSE18.10.11) *Pseudodictyomitra pseudomacrocephala* (SQUINABOL) (early Albian – early Turonian). 12) *Pseudodictyomitra pentacolaensis* (PESSAGNO) late Aptian – Coniacian). 13, 15-18) Sample CR-SE18.45. 13) *Pseudodictyomitra* sp. aff. *P.nakasekoi* TAKETANI. 14) (sample CR-SE18.25) *Pseudodictyomitra* sp. 15) *Pseudodictyomitra paronai* (ALIEV) (early Albian – early Cenomanian). 16) *Orbiculiforma railensis* PESSAGNO. 17) *Thanarla brouweri* (TAN) (latest Barremian – middle Albian). 18) *Diacanthocapsa fossilis* (SQUINABOL) (late Aptian – middle Cenomanian).